JOURNAL OF VIROLOGY, Oct. 2008, p. 9458–9464 Vol. 82, No. 19
0022-538X/08/$08.00+0 doi:10.1128/JVI.00647-08

Crystal Structure of Coxsackievirus B3 3D^{pol} Highlights the Functional Importance of Residue 5 in Picornavirus Polymerases$^{\nabla}$

Grace Campagnola, Mark Weygandt, Kirsten Scoggin, and Olve Peersen*

Department of Biochemistry and Molecular Biology, 1870 Campus Delivery, Colorado State University, Fort Collins, Colorado 80523-1870

Received 22 March 2008/Accepted 10 July 2008

The crystal structure of the coxsackievirus B3 polymerase has been solved at 2.25-Å resolution and is shown to be highly homologous to polymerases from poliovirus, rhinovirus, and foot-and-mouth disease viruses. Together, these structures highlight several conserved structural elements in picornaviral polymerases, including a proteolytic activation-dependent N-terminal structure that is essential for full activity. Interestingly, a comparison of all of the picornaviral polymerase structures shows an unusual conformation for residue 5, which is always located at a distortion in the β-strand composed of residues 1 to 8. In our earlier structure of the poliovirus polymerase, we attributed this conformation to a crystal packing artifact, but the observation that this conformation is conserved among picornaviruses led us to examine the role of this residue in further detail. Here we use coxsackievirus polymerase to show that elongation activity correlates with the hydrophobicity of residue 5 and, surprisingly, more hydrophobic residues result in higher activity. Based on structural analysis, we propose that this residue becomes buried during the nucleotide repositioning step that occurs prior to phosphoryl transfer. We present a model in which the buried N terminus observed in all picornaviral polymerases is essential for stabilizing the structure during this conformational change.

The picornaviruses are a family of small positive-strand RNA enteroviruses responsible for a wide range of ailments, including poliomyelitis, the common cold, and hepatitis A in humans and foot-and-mouth disease in livestock. The coxsackieviruses are a group of picornaviruses that commonly cause mild fever, aches, and conjunctivitis, as well as the more severe hand, foot, and mouth disease in children and viral heart disease in adults. These viruses are closely related to poliovirus based on phylogenetic analysis indicating that poliovirus emerged from type A coxsackieviruses and the observation that chimeric viruses with poliovirus capsid and coxsackievirus nonstructural proteins replicate efficiently (11).

The small ~7.5-kb picornaviral genomes encode a ~250-kDa polyprotein that is cleaved to produce several individual proteins, the last of which is an RNA-dependent RNA polymerase (RdRp). Known as 3D^{pol}, this enzyme carries out both initial negative-strand and subsequent positive-strand RNA synthesis and is essential for viral viability. The structures of polymerases from several families of viruses have been solved, and they show a common overall fold where the enzyme has palm, thumb, and fingers domains arranged as if in a right hand (6). In RdRps the tip of the fingers domain makes contact with the tip of the thumb, enclosing the active site located in the middle of the palm domain. This creates a channel through which NTPs enter the active site, while the RNA is located at the front of the polymerase with the template entering from the down along the fingers domain and the product duplex exiting along the thumb (6).

One unique aspect of many picornaviral polymerases is that they are only active upon complete proteolytic processing to produce the 3D^{pol} enzyme from the viral polyprotein. The structure of poliovirus 3D^{pol} revealed that the N-terminal glycine residue of the fully processed polymerase is buried in a pocket at the base of the fingers domain (20), while it extends away from the protein and is part of a flexible interdomain linker in the structure of the 3CD^{pro} precursor protein (14). Based on a comparison with a partial 3D^{pol} structure in which the fingers domain was disordered (10), the buried N terminus of the complete 3D^{pol} forms four hydrogen bonds that act to reposition Asp238 in the active site for a 2.8-Å long hydrogen bonding interaction with the 2′ hydroxyl of the incoming NTP (20). Consistent with this hydrogen bonding role, alanine mutations at the N terminus that indirectly alter the positioning of Asp238 or an alanine mutation of Asp238 itself to remove the carboxylate group result in a loss of activity and loss of electron density for a bound NTP in crystallization experiments (20). The positioning of the Asp238 residue has also been shown to be important for polymerase activity and fidelity (9). However, a comparison of the recently solved poliovirus 3CD^{pro} structure with the poliovirus 3D^{pol} structure does not show a significant difference in the positioning of Asp238 (14), suggesting that the buried N terminus may be functioning in some other way to activate the enzyme and modulate its elongation activity.

In order to gain a better understanding of the molecular basis for 3D^{pol} activation and fidelity in picornaviruses, we set out to solve the crystal structure of the coxsackievirus B3 polymerase. Here we report that structure at a 2.25-Å resolution and use comparisons with other picornaviral polymerases to identify functionally important conserved and nonconserved regions of the polymerase structure. In particular, we identified an unusual structural distortion in the first five residues of the protein that is highly conserved among picornaviral 3D^{pol} structures and provides an additional explanation for the requirement of a buried N terminus for polymerase activity.

* Corresponding author. Mailing address: Department of Biochemistry and Molecular Biology, 1870 Campus Delivery, Colorado State University, Fort Collins, CO 80523-1870. Phone: (970) 491-0433. Fax: (970) 491-0494. E-mail: Olve.Peersen@ColoState.edu.

$^{\nabla}$ Published ahead of print on 16 July 2008.

MATERIALS AND METHODS

Protein purification. Coxsackievirus B3 3D^{pol} with a C-terminal GSSSHH HHHH tag was expressed using the pKK-T7E vector in *Escherichia coli* BL21(DE3)/pLysS cells, as previously described for poliovirus polymerase (20). The cells were lysed by sonication and centrifuged at 17,000 rpm in a SS-34 rotor, and the clarified lysate was loaded onto a nickel charged chelating fast-flow Sepharose column (GE Healthcare), followed by step elution with 350 mM imidazole in 50 mM Tris (pH 8.0), 400 mM NaCl, 5% glycerol, and 0.02% NaN_3. Fractions containing the polymerase were pooled and diluted to reduce the NaCl concentration to ~0.1 M prior to loading onto a Q-Sepharose column and eluting with a linear gradient to 1 M NaCl with 25 mM Tris (pH 8.5), 15% glycerol, 0.02% (wt/vol) NaN_3, and 2 mM dithiothreitol (DTT). To prevent protein aggregation, the final salt concentration of fractions containing the polymerase was increased to 400 mM by the addition of 5 M NaCl. The pooled fractions were concentrated to ~0.8 ml and run over a Superdex 200 16/60 gel filtration column equilibrated in 400 mM NaCl, 5 mM Tris (pH 7.5), 0.02% (wt/vol) NaN_3, and 2 mM TCEP reducing agent (Pierce). The final yield is ~7 mg of purified protein per liter of bacterial culture.

Protein mutagenesis. All mutants were generated in the expression plasmid by using QuikChange mutagenesis protocol (Stratagene), confirmed by sequencing, and purified by the same protocol as the wild-type protein. Extinction coefficients were calculated based on the sequence using the ExPASy ProtParam program (http://www.expasy.ch/tools/protparam.html).

Activity assays. Poly(A)-oligo(dT) polymerase extension reactions (20 μl) containing 75 nM 3D^{pol}; 0.01 μg of poly(A) template (average length, 300 nucleotides)/μl; 0.005 μg of oligonucleotide dT_{15}/μl; 50 mM HEPES (pH 7.5); 25 μM UTP; 0.5 mM concentrations (each) of GTP, CTP, and ATP; 4 mM DTT; 1.5 mM magnesium acetate; 60 μM $ZnCl_2$; 0.1% NP-40; and 0.01 μCi of [α-^{32}P]UTP/μl were assembled on ice in a 96-well microtiter plate. The entire plate was then transferred onto a 30°C heatblock for the elongation reaction that was quenched at 3-min intervals between 6 and 24 min. Each protein or replicate sample occupies an entire eight-well column of the plate so that multiple time points can easily be quenched by adding 30 μl of 0.5 mM EDTA to an entire row of the plate using a multichannel pipettor. The incorporation of [^{32}P]uracil radiolabel was evaluated by filtering ~35 μl of the quenched reactions through a Hybond-N$^+$ nylon membrane supported on Whatman paper in a Schleicher & Schuell 96-well dot blot filter apparatus. The membrane was washed both before and after addition of the reaction with 25 mM MES (morpholineethanesulfonic acid; pH 6.5), 2.5 mM magnesium acetate, 40 μM $ZnCl_2$, 10% glycerol (vol/vol), and 2 mM DTT. The amount of radiolabeled RNA bound to the membrane was quantified by using a phosphorimager, and the activities were determined by linear regression of the radiolabel signal versus the reaction time. Comparison of the slopes of these linear ^{32}P incorporation curves yielded activities of the mutant proteins relative to wild-type 3D^{pol} controls that were always performed at the same time using the same reagents.

Tryptophan fluorescence. Fluorescence data were obtained by using an Aviv Instruments model ATF-105 spectrofluorometer with a 3-mm pathlength quartz cell containing 3D^{pol} at ~1.0 μM concentration in 25 mM HEPES (pH 7.5), 50 mM NaCl, and 10% glycerol. Emission scans from 300 to 450 nm (2-nm bandwidth) were collected with an excitation wavelength of 282 nm (4-nm bandwidth), and all experiments were performed at 20°C. The fluorescence spectra were background corrected using a buffer-only spectrum, and the concentration was normalized based on actual sample absorbance at 280 nm and the appropriate extinction coefficients (see Fig. 2). The actual protein concentrations thus determined ranged from 0.86 to 1.12 μM.

Structure determination. Crystals were grown by hanging-drop vapor diffusion at 16°C using 5 to 8 mg of protein/ml and precipitant solution containing 1.5 M ammonium sulfate and 25% glycerol. The crystals were harvested and frozen in liquid nitrogen without additional cryoprotectant. Diffraction data for coxsackievirus 3D^{pol} were collected at the MBC beamline 4.2.2 (Advanced Light Source, Berkeley, CA) and processed using the d*TREK suite of programs (16). The initial structure solution was obtained by molecular replacement using CNS (4) with the poliovirus polymerase structure as the search model; residues were then manually mutated to those found in coxsackievirus 3D^{pol}, and model bias was removed with a 2500K simulated annealing refinement. Several rounds of manual model rebuilding and refinement were performed using O (12) and CNS with the maximum likelihood intensity target. The figures were generated with the Pymol Molecular Graphics System (5), and structures were superimposed with all Cα atoms by using a maximum-likelihood-based approach implemented in the program Theseus (http://www.theseus3d.org) (17, 18). The crystallographic details are presented in Table 1.

TABLE 1. Crystallographic details

Parameter	Value
PDB[a] code	3DDK
Space group	$P4_32_12$
Unit cell (Å)	a = b = 74.36, c = 288.05
X-ray source	ALS 4.2.2 at 1.0 Å
Resolution limits (Å)	52.6–2.25 (2.33–2.25)
Reflections	
Total no. collected	326,269
No. unique	35,017
Redundancy	9.32 (1.78)
I/sigma	33.0 (3.0)
Completeness (%)	88.5 (41.4)
R_{merge} (%)	5.1 (24.3)
Refinement	
Resolution range (Å)	55–2.25
R (%)	20.1
R_{free} (%) (9.7% of data)	23.4
Model statistics	
No. of atoms (waters)	3,991 (262)
Avg B-factor	35.7 (40.8 for waters)
RMSD bond length (Å)	0.006
RMSD bond angle (°)	1.3
Ramachandran statistics	
Favored	370
Allowed	37
Generous	0
Disfavored	1

[a] PDB, Protein Data Base.

RESULTS

Structural overview. Coxsackievirus polymerase adopts the normal "right-hand" structure of an RdRp composed of fingers, palm, and thumb domains where the fingers domain contacts the top of the thumb to create an enclosed active site (Fig. 1A). Overall, the structure is essentially identical to those of the poliovirus (20) and rhinovirus polymerases (13), reflecting the strong structure and sequence homology among these viruses. Coxsackievirus 3D^{pol} retains the five distinct finger motifs used to describe poliovirus 3D^{pol} where the index finger contacts the thumb and the ring finger passes under the index finger to form the roof of the NTP entry channel leading to the active site (20). The enclosed active-site conformation is anchored by hydrophobic interactions between Phe30 and Phe34 of the index finger that insert into a groove at the top of the thumb domain and wrap around Trp404 in a structure homologous to that found to be important for the thermal stability of poliovirus polymerase (19). The major difference between the coxsackievirus and poliovirus polymerases is the presence of one extra residue in the coxsackie protein (Fig. 1B). This extra residue is inserted in a surface-exposed loop (residues 257 to 263) between two helices at a location corresponding to the knuckle of the ring finger when using the analogy of a right hand to describe the structure. This loop is also the site of one residue deletions in the rhinovirus polymerases compared to poliovirus 3D^{pol}, suggesting some structural variation can be tolerated in this region of the proteins (Fig. 1B).

N-terminal structure. The N-terminal Gly1 residue of coxsackievirus 3D^{pol} is buried in a pocket at the base of the fingers domain in a structure that is similar to those observed in other picornaviral polymerases. To test the importance of the N-terminal amino acids for enzyme activity, we generated a series

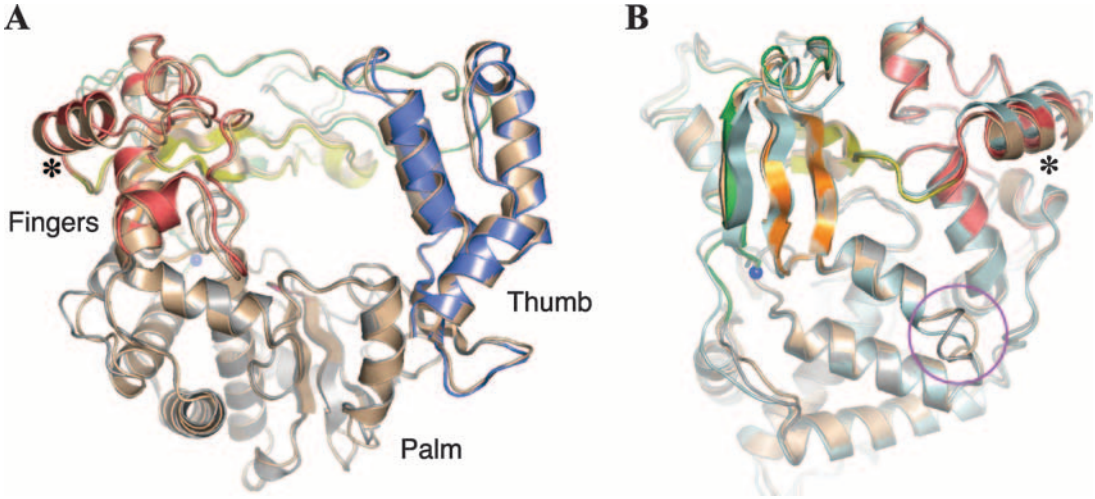

FIG. 1. Comparison of picornaviral polymerase structures. (A) Structures of coxsackievirus (multicolored) and poliovirus (tan) polymerases superimposed using a maximum-likelihood alignment of all Cα atoms that inherently emphasizes the palm domain, the most conserved part of the structure (18). (B) Superposition of the coxsackievirus, poliovirus (tan), and rhinovirus (light blue) polymerases showing the strong structural conservation of these enzymes and the single site of insertions and deletions in their sequences (magenta circle). The CV $3D^{pol}$ structure is colored with the convention previously used for poliovirus $3D^{pol}$ (20); palm in gray, thumb in blue, index finger in green, middle finger in orange, ring finger in yellow, and pinky finger in red. The N terminus of the CV protein is shown as a blue sphere. The view is from the left side of panel A, and the same helix is marked with an asterisk in both panels as a visual guide.

of mutants that altered the N terminus by adding or deleting single residues (Table 2). The mutant proteins were expressed in bacteria, and all were purified normally with the same elution profile as the wild-type protein from gel filtration chromatography, indicating that there is no major structural perturbation as a result of these mutations. As was observed for poliovirus polymerase (20), there is a complete loss of polymerase activity in the poly(A) template assay as a result of either deleting the N-terminal Gly1 residue or adding a glutamine residue, the last residue in the $3C^{pro}$ protein. We also further examined the role of the N-terminal Gly1 residue by adding a second glycine residue to the N terminus. Surprisingly, this also resulted in a mutant that showed a complete loss of activity despite having a glycine as its first residue. We then tested whether this result was simply due to starting the protein with two consecutive glycine residues by mutating Glu2 to a glycine. This mutant retained 11% of wild-type activity, showing that a Gly-Gly N-terminal sequence reduces, but does not totally abolish, elongation activity.

TABLE 2. Activities of coxsackievirus $3D^{pol}$ mutants[a]

Initial protein	Activity sequence[b]	Activity (mean % of WT ± SD)
WT	GEIE**F**IEE...	100 ± 3
ΔG1	EIE**F**IEE...	0.8 ± 0.3
+Q	QGEIE**F**IEE...	1.5 ± 0.3
+G	GGEIE**F**IEE...	1.5 ± 0.7
E2G	GGIE**F**IEE...	11 ± 3
F5W	GEIE**W**IEE...	160 ± 30
F5L	GEIE**L**IEE...	79 ± 6
F5I	GEIE**I**IEE...	35 ± 4
F5V	GEIE**V**IEE...	16 ± 2
F5A	GEIE**A**IEE...	4.2 ± 1.2
F5D	GEIE**D**IEE...	2.4 ± 0.2
Y62H		2.6 ± 0.3
F5D+Y62H		0.6 ± 0.1

[a] WT, wild type.
[b] The mutation sites are underlined, and residue 5 is indicated in boldface.

β-Strand distortion at Phe5. The $3D^{pol}$ structure begins with the buried N terminus and the first four residues being hydrogen bonded to the middle finger motif in a canonical antiparallel β-sheet conformation. However, the secondary structure then diverges from the normal β-strand geometry and hydrogen bonding pattern so as to expose residue Phe5 on the surface of the protein before continuing with canonical β-strand hydrogen bonding for residues 6 through 9 (see Fig. 3). Interestingly, this distortion is present in all of the picornaviral $3D^{pol}$ structures, indicating it is a conserved feature that may have a functional role in these polymerases (8, 13, 20). We wanted to investigate the importance of this residue in greater detail and therefore made a series of five mutations at Phe5 in coxsackievirus $3D^{pol}$ and assayed the resulting purified proteins for elongation activity.

The nature of residue 5 has a profound effect on enzyme activity, which correlates with the size and hydrophobicity of the amino acid at this position (Table 2). When the native Phe5 is mutated to a larger tryptophan the enzymatic activity increased to >1.5-fold that of the wild type, while mutations to smaller residues such as leucine, isoleucine, valine, and alanine result in activities being reduced 1.3- to ~25-fold. Tryptophan fluorescence difference spectra comparing the Phe5Trp and wild-type proteins show that the mutated Trp5 residue has a fluorescence emission maximum at ~350 nm, a finding consistent with the residue being solvent exposed (Fig. 2). In the foot-and-mouth disease virus polymerase structure (8) there is an unique arrangement of residues where residue 5 is a negatively charged aspartic acid and residue 64 is a histidine, two residues that could potentially form a salt bridge if Asp5 were

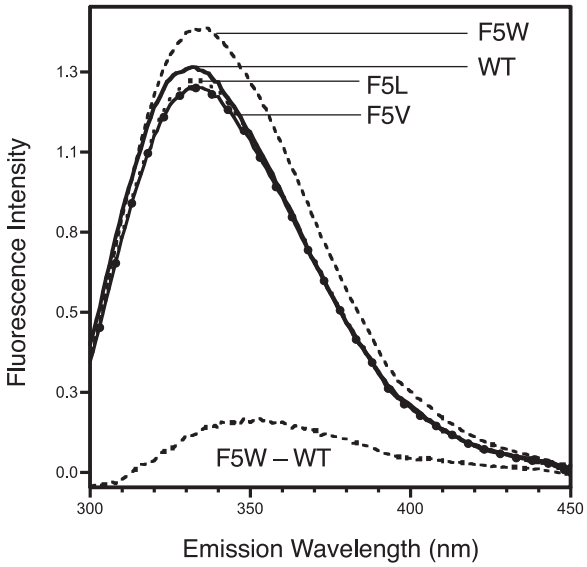

FIG. 2. Tryptophan fluorescence spectra of wild-type coxsackievirus 3D^{pol} and the F5W, F5L, and F5V mutants. The F5W–wild-type difference spectrum shows that the introduced Trp5 residue has a peak at ~350 nm that is indicative of a solvent-exposed tryptophan whose total intensity is consistent with adding an eighth Trp residue to seven already found in the protein. Spectra were collected using ~1 μM protein and normalized to the exact protein concentration based on sample absorbance (range, 0.86 to 1.12 μM).

to become buried during the catalytic cycle. In contrast, the structurally equivalent residue is highly conserved as a hydrophobic Tyr62 in coxsackievirus, poliovirus, and rhinovirus polymerases. We tested whether the alternative arrangement of residues could be functional in coxsackievirus 3D^{pol} by making the two mutants (F5D and Y62H) individually and as a double mutation. The two single mutants resulted in ~40-fold reductions in activity compared to the wild type, while the double mutant reduced activity ~170-fold (Table 2). Thus, there was no indication of compensatory behavior when these point mutations were introduced in the coxsackie 3D^{pol} background.

DISCUSSION

The structure of coxsackievirus B3 polymerase is quite similar to those of poliovirus and three rhinovirus polymerases, and together these picornaviral structures highlight several structurally conserved motifs (Fig. 1). All of the structures adopt the "right-hand" conformation commonly used to describe polymerases and feature the enclosed active site topology common to RdRps where the fingers domain reaches over the palm domain to make contact with the top of the thumb domain (20). This creates a tunnel through which NTPs access the active site and pyrophosphate is released. The RNA template strand enters the active site from the top of the polymerase through a channel between the pinky finger and thumb, and the RNA duplex exits along the thumb domain, as shown by several structures of the homologous foot-and-mouth disease 3D^{pol} elongation complexes (7, 8) and the related Norwalk virus 3D^{pol}-RNA complex (21).

The major structural difference between the coxsackievirus and poliovirus polymerases is the presence of one extra residue in the coxsackievirus protein. This extra residue is inserted in a surface-exposed loop composed of residues 257 to 263 between two helices at a location corresponding to the knuckle of the ring finger when using the analogy of a right hand to describe the structure (Fig. 1B). Interestingly, this region of the polymerase domain has been implicated in the recruitment of membrane trafficking Arf GTPases and associated guanine nucleotide exchange factors during poliovirus infection (3). This recruitment is by the poliovirus 3CD^{pro} protein where Arf binding is affected by mutations at Phe441, which corresponds to Phe258 in 3D^{pol} that is located in this variable loop and buried up against the palm domain. The structure of poliovirus 3CD^{pro} shows that the conformations of the individual 3C^{pro} and 3D^{pol} domains remain intact in the precursor (14), and thus we fully expect that this loop insertion difference between the poliovirus and coxsackievirus proteins also exists in 3CD^{pro}. Furthermore, the 257-263 loop is also the site of a one-residue deletion in the rhinoviral polymerases and a two-residue insertion in foot-and-mouth disease virus 3D^{pol} compared to the poliovirus protein. It appears that structure and sequence variation are well tolerated in this region of the 3D^{pol}, and it may represent a patch on the picornaviral polymerase surface that is universally available for host protein interactions.

Using coxsackievirus 3D^{pol}, we further investigated two highly conserved aspects of the picornaviral polymerase structures: the role of the buried N terminus in activating the polymerase upon cleavage from the 3CD^{pro} precursor protein and the role of an intriguing conserved structural distortion around residue Phe5 in modulating enzyme activity. The proteolytic processing of the 3CD^{pro} protein into separate 3C^{pro} and 3D^{pol} molecules is crucial for the activation of the polymerase enzyme in many picornaviruses. We have earlier shown that additions and deletions of even a single residue at the N terminus of poliovirus 3D^{pol} abolished enzymatic activity, and mutations of the Gly1 residue to larger alanine and serine residues reduce polymerase activity to ~50 and ~2%, respectively (20). Here we made similar addition and deletion mutations in coxsackievirus 3D^{pol} and showed that they also abolish elongation activity in this enzyme (Table 2). We also tested whether or not the enzyme could accommodate an additional glycine residue at the N terminus. Surprisingly, this glycine addition mutant was also essentially inactive (1.5%), indicating that the N-terminal sequence requirement for polymerase activation is not solely having a N-terminal glycine residue. One possible explanation for this is that starting the protein sequence with two very flexible glycine residues does not allow proper burial of the N terminus and subsequent positioning of Asp238 for interactions with the bound NTP. To address this, we mutated Glu2 to a glycine, thus retaining the normal length of the protein while starting with a Gly-Gly sequence, and we observed 11% of wild-type activity from this mutant (Table 2). Based on these results, it seems that the N-terminal residue itself as well as the specific sequence at the start of the protein are both important for enzymatic activity.

In this regard, one striking feature of all of the picornaviral polymerase structures is the conservation of a distortion in the β-strand conformation adopted by the first nine residues of the protein as they form an antiparallel β-sheet with the middle finger motif (Fig. 3). This distortion is a simple break of the

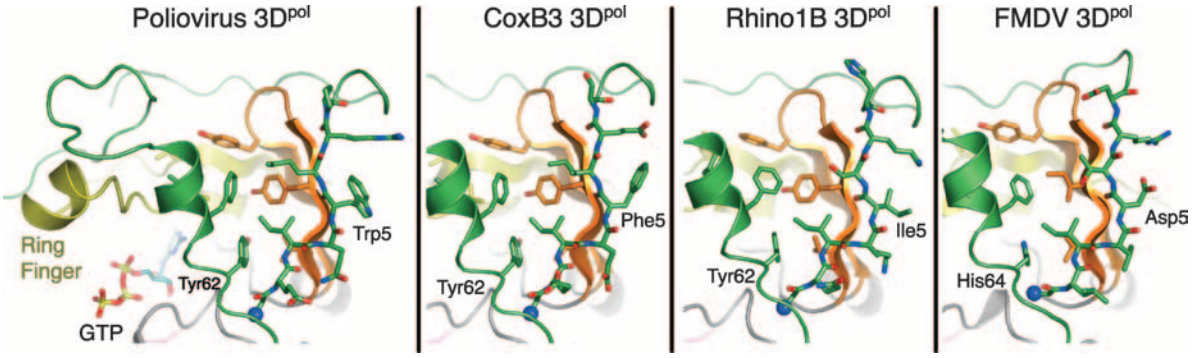

FIG. 3. Structural conservation of surface-exposed residue 5 in picornaviral polymerases. The structures of poliovirus $3D^{pol}$ with a bound GTP (PDB code 1RA7), coxsackievirus B3 (3DDK), rhinovirus 1B (1XR6), and foot-and-mouth disease virus (1U09) polymerases are shown in identical views from the back of the polymerase using the same domain coloring scheme as in Fig. 1. Residue 5 is labeled in each structure, as is the location of Tyr62 in poliovirus, coxsackievirus, and rhinovirus $3D^{pol}$ and the structurally equivalent His64 in foot-and-mouth disease virus polymerase.

β-sheet hydrogen bonding register such that the fifth residue in the protein, which is typically hydrophobic, becomes exposed on the outside surface of the protein rather than being buried toward the inside as it would in a canonical β-strand. In our earlier work on the structure of poliovirus polymerase (20) we attributed this conformation to a crystal packing artifact involving the surface exposed Trp5 residue interacting with another polymerase in the lattice and hypothesized that Trp5 should be tucked into the large exposed hydrophobic patch between the index and middle finger motifs (Fig. 3). Such a conformation would allow residues 1 to 9 to form a canonical β-strand structure with amino acids alternating on opposite sides of the strand and result in the formation of an antiparallel β-sheet with the middle finger motif. We were thus surprised to see the same "flipped-out" conformation of Phe5 in the coxsackie $3D^{pol}$ structure, and a further analysis of the $3D^{pol}$ structures from rhinoviruses (13) and foot-and-mouth disease virus (8) revealed that this flipped out conformation for residue 5 is conserved among picornaviral polymerases (Fig. 3). Such a high level of structural conservation suggests that the unusual conformation of residue 5 is functionally important in these polymerases.

To examine this in further detail, we made a series of mutations at Phe5 in coxsackievirus $3D^{pol}$ and tested the resulting proteins for poly(A) templated elongation activity. The results show a clear correlation between residue hydrophobicity and enzymatic activity; mutation to a larger tryptophan residue, as is found in poliovirus polymerase, increases activity, whereas mutations to smaller residues, such as isoleucine found in the rhinoviral polymerases, reduce activity (Table 2). The tryptophan fluorescence spectrum of the Phe5Trp mutant coxsackie $3D^{pol}$ protein shows that the newly introduced Trp5 residue has an emission maximum at ~350 nm, a finding consistent with it being solvent exposed in the Apo form of the protein (Fig. 2). The finding that more hydrophobic residues have higher activities suggests that residue 5 becomes buried at some point in the catalytic cycle, with the larger residues providing more driving force for a conformational change that in turn increases the enzymatic turnover rate.

Although the structural changes associated with this conformational change are not yet known, a prime candidate is the NTP repositioning step where the nucleotide is moved from its initial binding site into the correct geometry for catalysis upon proper base pairing. This is a rate-limiting step in the poliovirus $3D^{pol}$ catalytic cycle (1), where the structures of $3D^{pol}$-NTP complexes reveal that nucleotides are initially bound in a preinsertion site and the ring finger motif of $3D^{pol}$ is likely involved in a subsequent NTP repositioning step (19). In light of this, if we model the first nine residues of $3D^{pol}$ in a canonical β-strand conformation, i.e., without the distortion, then residue 5 will become buried in the large hydrophobic cavity whose bottom is in direct contact with the ring finger. A movement of the ring finger to reposition the NTP would likely involve a rearrangement of this hydrophobic cavity, and it is therefore quite plausible that the size and hydrophobicity of residue 5 could play an important role in stabilizing such a conformational change. This model provides a molecular explanation for the activity effects arising from our Phe5 mutations.

We have previously implicated the buried N terminus and Gly1 residue as being involved in positioning Asp238 in the active site to form a 2.8-Å hydrogen bond with the 2′ hydroxyl of the incoming NTP molecule (20). This new model for the initial conformational change to reposition the NTP for catalysis provides a second explanation for the importance of proteolytic processing and burying the N terminus in order to activate the picornaviral polymerases: if residue 5 were to flip from an exposed to a buried conformation during the catalytic cycle, then some of the β-sheet hydrogen bonding interactions involving residues 1 to 4 or residues 6 to 8 would have to be disrupted so that residue 5 could rotate into the buried position. In the native $3D^{pol}$ structure there are a total of seven hydrogen bonds that lock in the conformation of the buried N terminus and residues 1 to 4, while there are only four hydrogen bonds for residues 6 to 8 (Fig. 4A). With this in mind, we propose that one step in the $3D^{pol}$ catalytic cycle involves a fraying of the top end of the β-strand, releasing residues 6 to 8 such that residue 5 can be flipped into a buried conformation. For this coordinated movement to occur, it is imperative that the bottom portion of the index finger remains "locked" in position because it serves as a stable anchor for the pivot movement of residue 5. This is the point at which proper proteolytic processing is critically important because the proper anchoring of residues 1 to 4 via the seven hydrogen

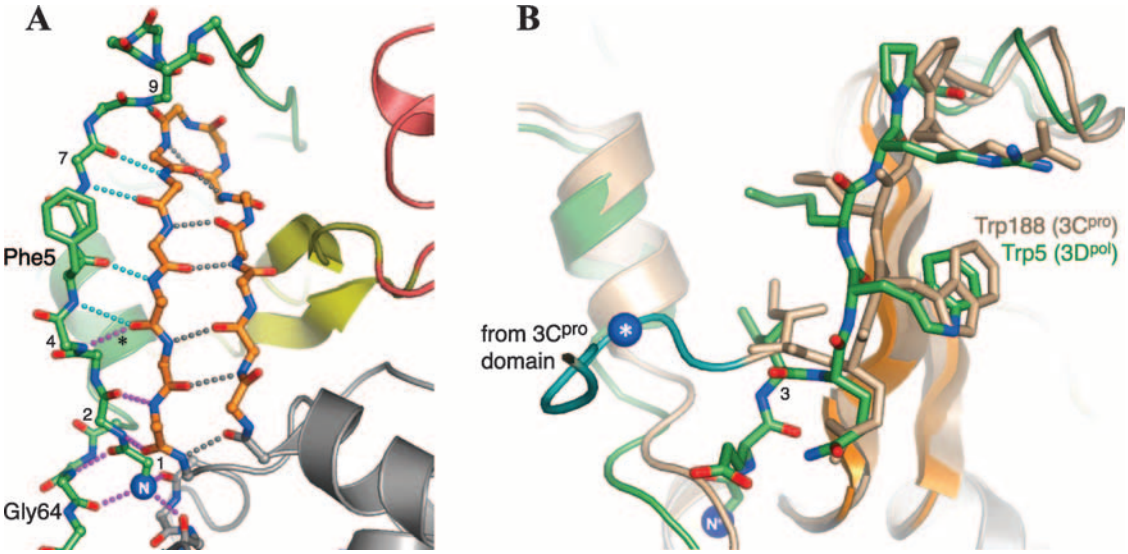

FIG. 4. Interactions surrounding the polymerase N termini in 3D^{pol} and 3CD^{pro} structures. (A) Coxsackievirus 3D^{pol} structure showing the hydrogen bonding interactions surrounding the buried N terminus and initial β-strand. In this structure there are seven hydrogen bonds (magenta) involving residues 1 to 4 that would serve to anchor the N-terminal sequence and four hydrogen bonds (cyan) that would have to be broken in order to undergo the proposed conformational change to bury residue 5 during NTP repositioning. (B) Comparison of the poliovirus 3D^{pol} (multicolor) and 3CD^{pro} (tan) structures at the polyprotein junction showing how the polymerase domain structures are essentially identical starting at residue Ile3. The lack of the 3D^{pol} N terminus in the uncleaved precursor protein means that the first two residues of the polymerase become part of the flexible interdomain linker between the 3C^{pro} and 3D^{pol} domains (cyan with a blue sphere marking the position of the polymerase domain Gly1 amino group). As a result, only one of the seven N-terminal hydrogen bonds found in 3D^{pol} is formed in the 3CD^{pro} structure (marked with an asterisk in panel A). The superpositioning of the 3D^{pol} and 3CD^{pro} structures was based on the entire polymerase domain and is dominated by the palm structure (as shown in Fig. 1), resulting in a slight rotational offset between 3D^{pol} and 3CD^{pro} in this region of the structures.

bonds can only occur if the N terminus has been properly generated and buried in the structure.

This model explains the lack of activity from our coxsackievirus 3D^{pol} mutant where we added an extra glycine residue to the N terminus (+G mutant in Table 2). In this mutant the spacing between the buried N terminus and the hydrophobic phenylalanine has increased by one residue (Table 2), and thus the proper conformational change cannot take place; the Phe5 residue has been shifted up the β-strand by one residue and is now effectively Phe6, which is located on the wrong side of the β-strand to interact with the hydrophobic patch. As predicted by our model, we can recover activity by then also deleting one residue to restore the wild-type spacing between Phe5 and the N terminus (Table 2, where the E2G mutation is equivalent to a +G/ΔGlu2 double mutant).

The structure of poliovirus 3CD^{pro} is also consistent with the model in that it shows 3D^{pol} and 3CD^{pro} diverging exactly at residue 3 of the 3D^{pol} domain (14); in this structure residues 1 and 2 of the 3D^{pol} domain extend away from the polymerase, while residues 3 to 8 have essentially the same conformation in the two proteins (Fig. 4B). According to our proposed conformational change model, we would attribute the lack of polymerase activity from 3CD^{pro} to its inability to anchor residues 1 to 4 in a conformation that would allow the NTP repositioning step to take place. In effect, any attempt by 3CD^{pro} to reposition a nucleotide for catalysis without such an anchor would simply result in the dissociation of residues 6 to 9 (and likely residues 3 to 9) from the rest of the 3D^{pol} domain, rather than a concerted conformational change to bury residue 5 and move the ring finger. Last, biochemical analysis of a poliovirus 3D^{pol} Gly64Ser mutant demonstrates a direct link between the structure stabilizing the buried N terminus and conformational changes during the catalytic cycle. Gly64 is a key residue that forms two hydrogen bonds with the buried Gly1 (Fig. 4A), and this mutant results in a polymerase with a slowed NTP repositioning step and higher fidelity (2, 15).

At this point we have two interpretations for how proteolytic cleavage leads to the activation of some picornaviral polymerases; our earlier model involving hydrogen bonding of Asp238 and the bound NTP (20), and the model presented here implicating a stabilizing effect during conformational changes to reposition the NTP for catalysis. There is compelling data for both models, and it is quite likely that they both play a role in modulating 3D^{pol} activity. The Asp238 repositioning model was initially based on a comparison of the complete poliovirus 3D^{pol} structure with a partial structure lacking the fingers domain (10), yet the recently determined structure of 3CD^{pro} suggests that this apparent shift in Asp238 may have been a crystallization artifact of that partial structure (14). However, our crystal soaking experiments shows that NTP binding, as judged by electron density, is critically dependent on forming a hydrogen bond between Asp238 and the 2′ hydroxyl of the NTP (19, 20). We observed very strong and unambiguous density for GTP bound to the wild-type protein but no density whatsoever under the same conditions when using an Asp238Ala mutant, a Gly1Ala mutant that repositions Asp238 so that the hydrogen bonding distance is too long (~4 Å), or upon soaking in 2′-deoxy GTP that is incapable of forming the hydrogen bond. Also, NTP repositioning is a rate-limiting step in the polymerase catalytic cycle, and the posi-

tioning of Asp238 is important for catalytic efficiency and fidelity (9), so it is not surprising that subtle alterations in this region of the structure have large effects on activity.

In closing, the structure of coxsackievirus $3D^{pol}$ highlights the strong structural conservation among picornaviral polymerases, including the buried N terminus that is required for proper function and proteolytic activation of these enzymes, an unusual backbone conformation around residue 5 that may be important the enzyme's catalytic cycle, and a site for insertions and deletions at the base of the pinky finger that has been implicated in host protein interactions. Although the structure of an active picornaviral polymerase elongation complex that explicitly shows the conformational changes associated with nucleotide repositioning for catalysis remains elusive, we can at this point gain much from structural and functional comparisons of these highly homologous proteins.

ACKNOWLEDGMENTS

We thank Peng Gong and Sarah Hobdey for comments on the manuscript and Bert Semler and Steven Tracy for providing clones of the coxsackievirus B3 polymerase.

This study was supported by NIH grant R01-AI059130.

REFERENCES

1. **Arnold, J. J., and C. E. Cameron.** 2004. Poliovirus RNA-dependent RNA polymerase ($3D^{pol}$): pre-steady-state kinetic analysis of ribonucleotide incorporation in the presence of Mg^{2+}. Biochemistry **43:**5126–5137.
2. **Arnold, J. J., M. Vignuzzi, J. K. Stone, R. Andino, and C. E. Cameron.** 2005. Remote site control of an active site fidelity checkpoint in a viral RNA-dependent RNA polymerase. J. Biol. Chem. **280:**25706–25716.
3. **Belov, G. A., C. Habbersett, D. Franco, and E. Ehrenfeld.** 2007. Activation of cellular Arf GTPases by poliovirus protein 3CD correlates with virus replication. J. Virol. **81:**9259–9267.
4. **Brunger, A. T., P. D. Adams, G. M. Clore, W. L. DeLano, P. Gros, R. W. Grosse-Kunstleve, J. S. Jiang, J. Kuszewski, M. Nilges, N. S. Pannu, R. J. Read, L. M. Rice, T. Simonson, and G. L. Warren.** 1998. Crystallography and NMR system: a new software suite for macromolecular structure determination. Acta Crystallogr. D Biol. Crystallogr. **54**(Pt. 5)**:**905–921.
5. **DeLano, W. L.** 2002. The PYMOL molecular graphics system. DeLano Scientific, San Carlos, CA.
6. **Ferrer-Orta, C., A. Arias, C. Escarmis, and N. Verdaguer.** 2006. A comparison of viral RNA-dependent RNA polymerases. Curr. Opin. Struct. Biol. **16:**27–34.
7. **Ferrer-Orta, C., A. Arias, R. Perez-Luque, C. Escarmis, E. Domingo, and N. Verdaguer.** 2007. Sequential structures provide insights into the fidelity of RNA replication. Proc. Natl. Acad. Sci. USA **104:**9463–9468.
8. **Ferrer-Orta, C., A. Arias, R. Perez-Luque, C. Escarmis, E. Domingo, and N. Verdaguer.** 2004. Structure of foot-and-mouth disease virus RNA-dependent RNA polymerase and its complex with a template-primer RNA. J. Biol. Chem. **279:**47212–47221.
9. **Gohara, D. W., J. J. Arnold, and C. E. Cameron.** 2004. Poliovirus RNA-dependent RNA polymerase ($3D^{pol}$): kinetic, thermodynamic, and structural analysis of ribonucleotide selection. Biochemistry **43:**5149–5158.
10. **Hansen, J. L., A. M. Long, and S. C. Schultz.** 1997. Structure of the RNA-dependent RNA polymerase of poliovirus. Structure **5:**1109–1122.
11. **Jiang, P., J. A. Faase, H. Toyoda, A. Paul, E. Wimmer, and A. E. Gorbalenya.** 2007. Evidence for emergence of diverse polioviruses from C-cluster coxsackie A viruses and implications for global poliovirus eradication. Proc. Natl. Acad. Sci. USA **104:**9457–9462.
12. **Jones, T. A., J. Y. Zou, S. W. Cowan, and M. Kjeldgaard.** 1991. Improved methods for building protein models in electron density maps and the location of errors in these models. Acta Crystallogr. A **47:**110–119.
13. **Love, R. A., K. A. Maegley, X. Yu, R. A. Ferre, L. K. Lingardo, W. Diehl, H. E. Parge, P. S. Dragovich, and S. A. Fuhrman.** 2004. The crystal structure of the RNA-dependent RNA polymerase from human rhinovirus: a dual function target for common cold antiviral therapy. Structure **12:**1533–1544.
14. **Marcotte, L. L., A. B. Wass, D. W. Gohara, H. B. Pathak, J. J. Arnold, D. J. Filman, C. E. Cameron, and J. M. Hogle.** 2007. Crystal structure of poliovirus 3CD protein: virally encoded protease and precursor to the RNA-dependent RNA polymerase. J. Virol. **81:**3583–3596.
15. **Pfeiffer, J. K., and K. Kirkegaard.** 2003. A single mutation in poliovirus RNA-dependent RNA polymerase confers resistance to mutagenic nucleotide analogs via increased fidelity. Proc. Natl. Acad. Sci. USA **100:**7289–7294.
16. **Pflugrath, J. W.** 1999. The finer things in X-ray diffraction data collection. Acta Crystallogr. D Biol. Crystallogr. **55**(Pt. 10)**:**1718–1725.
17. **Theobald, D. L., and D. S. Wuttke.** 2006. Empirical Bayes hierarchical models for regularizing maximum likelihood estimation in the matrix Gaussian Procrustes problem. Proc. Natl. Acad. Sci. USA **103:**18521–18527.
18. **Theobald, D. L., and D. S. Wuttke.** 2006. THESEUS: maximum likelihood superpositioning and analysis of macromolecular structures. Bioinformatics **22:**2171–2172.
19. **Thompson, A. A., R. A. Albertini, and O. B. Peersen.** 2007. Stabilization of poliovirus polymerase by NTP binding and fingers-thumb interactions. J. Mol. Biol. **366:**1459–1474.
20. **Thompson, A. A., and O. B. Peersen.** 2004. Structural basis for proteolysis-dependent activation of the poliovirus RNA-dependent RNA polymerase. EMBO J. **23:**3462–3471.
21. **Zamyatkin, D. F., F. Parra, J. M. Martin Alonso, D. A. Harki, B. R. Peterson, P. Grochulski, and K. K. Ng.** 2008. Structural insights into mechanisms of catalysis and inhibition in norwalk virus polymerase. J. Biol. Chem. **283:**7705–7712.